Eigenmodes of surface energies for shape analysis

Klaus Hildebrandt, Christian Schulz, Christoph von Tycowicz, and Konrad Polthier

Freie Universität Berlin

Abstract. In this work, we study the spectra and eigenmodes of the Hessian of various discrete surface energies and discuss applications to shape analysis. In particular, we consider a physical model that describes the vibration modes and frequencies of a surface through the eigenfunctions and eigenvalues of the Hessian of a deformation energy, and we derive a closed form representation for the Hessian (at the rest state of the energy) for a general class of deformation energies. Furthermore, we design a quadratic energy, such that the eigenmodes of the Hessian of this energy are sensitive to the extrinsic curvature of the surface.

Based on these spectra and eigenmodes, we derive two shape signatures. One that measures the similarity of points on a surface, and another that can be used to identify features of the surface. In addition, we discuss a spectral quadrangulation scheme for surfaces.

1   Introduction

The spectrum and the eigenfunctions of the Laplace-Beltrami operator of a surface have stimulated much recent work in shape analysis and geometry processing, ranging from parametrization, segmentation, and symmetry detection to shape signatures and mesh filtering. Such methods profit from the properties of the eigenfunctions of the Laplace-Beltrami operator. For example, on a curved surface they form an orthogonal basis of the space of L^2-functions on the surface. Furthermore, the Laplacian depends only on the metric of the surface, hence the eigenvalues and eigenfunctions are invariant under isometric deformations of the surface. However, there are disadvantages as well. For example, a consequence of the invariance to isometric deformations is an insensitivity to extrinsic feature of the surface, like sharp bends, that are of essential importance for some applications.

Contributions. In this work we derive operators, whose eigenmodes and spectra can serve as alternatives to the spectrum and modes of the Laplacian for applications in geometry processing and shape analysis. On the one hand, the eigenfunctions of these operators share properties with the eigenfunctions of the Laplacian, *e.g.*, they form an orthogonal basis of an adequate space of variations of the surface. On the other hand, there are fundamental differences, *e.g.*, these eigenfunctions depend (not only on intrinsic quantities but also) on the extrinsic curvature of the surface. We consider two different settings: vibration modes and frequencies of surfaces derived from deformation energies, and eigenvalues and

eigenmodes of the Hessian of quadratic energies that are defined on a space of functions on a surface.

On a planar domain, the eigenfunctions of the Laplacian serve as a model for the vibration modes of a flat plate (Chladni plates). For curved surfaces more elaborate models are required to describe the vibration modes of a surface. We consider a physical model that describes vibration modes of a surface mesh through the eigenfunctions of the Hessian of a deformation energy. In general, computing the Hessian of a deformation energy is a delicate and laborious task. But, to compute the vibration modes we do not need to compute the Hessian at all points in the space of possible surfaces, but only at the point that represents the reference surface. We derive a simple formula, that can be used to compute the Hessian at the reference surface for a general class of deformation energies. We hope that this framework will stimulate further exploration of the eigenmodes and eigenfrequencies of deformation energies.

The Dirichlet energy of a surface is a quadratic functional on an appropriate space of functions on a surface. The Hessian of this energy is the Laplace-Beltrami operator of the surface. We propose a quadratic functional that can be derived from the Dirichlet energy, but is not intrinsic. The eigenfunctions of this energy are sensitive to the extrinsic curvature of the surface.

We discuss three applications that use the proposed eigenmodes and spectra. We define two (multi-scale) signatures, the *vibration signature*, based on the vibration modes, and the *feature signature*, based on the eigenmodes of the modified Dirichlet energy. To each of the two signatures we associate a (multi-scale) pseudo-metric on the surface. The resulting *vibration distance* can be used as a similarity measure on the surface and the *feature distance* can identify features of a mesh. Furthermore, we test the *spectral surface quadrangulation* method of Dong et al. [6] with specific vibration modes, instead of eigenfunctions of the Laplacian. The resulting quadrangulation, in our opinion, aligns better with the extrinsic curvature of the surface.

Related work. Recently, we have seen a boom of papers that use the eigenvalues and eigenfunctions of the Laplace-Beltrami operator as an ingredient to algorithms in geometry processing and shape analysis. An overview of this development can be found in the recent survey by Zhang et al. [29] and in the course notes of a *Siggraph Asia 2009* course held by Lévy and Zhang [16]. Here, we can only briefly outline the work that has been most relevant for this paper.

The spectrum of the Laplace-Beltrami operator of a Riemannian manifold contains a significant amount of information about the manifold and the metric. Though it does not fully determine the Riemannian manifold, it can be used as a powerful shape descriptor of a class of isometric Riemannian manifolds. Reuter et al. [21, 22] use the spectrum of the Laplace-Beltrami operator to construct a finger print of surfaces, which they call the *Shape-DNA*. By construction this finger print is invariant under isometric deformations of a surface. Among other applications the Shape-DNA can be used for shape matching, copyright protection, and database retrieval. Rustamov [23] developed the *Global Point Signature (GPS)*, a signature that can be used to classify shapes up to isometry. Based
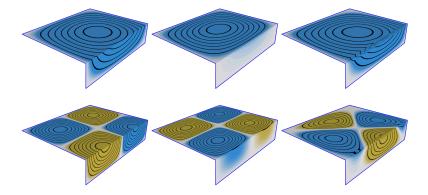
Fig. 1. Visualization of modes of different energies. First column shows the Laplacian eigenmodes, second column the eigenmodes of the modified Dirichlet energy E_D^N, and third column the vibrations modes derived from the thin shell energy restricted to normal variations.

on GPS, Ovsjanikov et al. [17] developed a method for the detection of global symmetries in shapes. Dong et al. [6] present an elegant technique that uses the Morse-Smale complex (and the quasi-dual complex) of a carefully chosen Laplace eigenfunction to generate a coarse quadrangulation of a surface mesh. This approach was extended by Huang et al. [14], who design a least-squares optimization routine that modifies the selected Laplace eigenfunction (and hence its Morse-Smale complex) and provides a user with control of the shape, size, orientation, and feature alignment of the faces of the resulting quadrangulation. The computation of the spectrum and eigenfunctions of the Laplacian is a delicate and computationally expensive task, even for medium sized meshes. Vallet and Lévy [27] propose an efficient shift-and-invert Lanczos method and present an implementation that is designed to handle even large meshes. Using the eigenfunctions of the Laplacian, one can compute the heat kernel of the surface. Sun et al. [26] propose a surface signature based on the heat kernel and use the signature to derive a measure for the geometric similarity of different regions of the surface. Due to its construction, this measure is invariant under isometric deformations of the surface. Independent of this work, Gebal et al. [10] propose a similar signature, named the *Auto Diffusion Function*, and use it for mesh skeletonization and segmentation.

Modal analysis is a well established technique in structural mechanics and mechanical engineering, that aims at computing the modes and frequencies of an object during vibration. In graphics, it is mainly used to speed up physical simulations, see [2, 4, 12, 18]. Recently, Huang et al. [15] use vibration modes of a surface to decompose it into physically meaningful parts. They compute the modes of the surface from the Hessian of the *as-rigid-as-possible* deformation energy, which was proposed by Sorkine and Alexa [25].

In physical simulation, thin shell models describe the dynamics of a thin flexible structure that has a curved undeformed configuration. For example, in cloth simulation thin shells are used to describe folds and wrinkles [3]. Common discrete models [1, 3, 9, 11] describe the middle surface of a thin shell by a mesh and measure the bending of the surface at the edges of the mesh. Of particular interest for this work is the model of Grinspun et al. [11] that uses a discrete energy to simulate thin shells.

2   Deformation Energies

In this section, we consider discrete deformation energies that are defined for surface meshes in $\mathbb{R}^3$. Such energies measure the deformation of a mesh from a reference mesh. A surface mesh is given by the positions of the vertices and the combinatorial information which vertices form triangles. Here, we vary only the positions of the vertices and leave the combinatorial information unchanged. The positions of the vertices can be written in one $3n$-vector x, where n is the number of vertices. Hence, we can identify the space of meshes (with fixed combinatorics) with $\mathbb{R}^{3n}$.

A general deformation energy. We consider deformation energies of the following form:

$$E(x) = \frac{1}{2} \sum_i \omega_i(\bar{x}) \left(f_i(x) - f_i(\bar{x}) \right)^2 , \qquad (1)$$

where x is a surface mesh and $\bar{x}$ a fixed reference mesh. In this equation, the sum can run over the edges, the vertices, or the triangles of x, and the f_i's and ω_i's are elementary functions, which *e.g.* measure angles, length of edges, or area of triangles. The weights ω_i must be positive and we require E to be twice continuously differentiable around $\bar{x}$. Then, E has global minimum at $\bar{x}$, which implies that the gradient of E at $\bar{x}$ vanishes and that the Hessian of E at $\bar{x}$ is positive semi-definite.

As an example of such an energy we consider a discrete energy that is designed for thin shell simulation.

Discrete shells. If we regard the surface mesh as a thin shell, then a physical model of thin shells provides us with a deformation energy. Here, we consider the discrete shell model of Grinspun et al. [11]. The energy that governs this model of thin shells is a weighted sum of two components: a flexural energy and a membrane energy. The weight reflects properties of the material to be simulated, *e.g.*, in cloth simulation the membrane energy usually gets a high weight due to the stretching resistance of cloth.

The discrete flexural energy is given as a summation over the edges of the mesh:

$$E_F = \frac{3}{2} \sum_i \frac{\|\bar{e}_i\|^2}{\bar{A}_{e_i}} \left(\theta_{e_i} - \bar{\theta}_{e_i} \right)^2 , \qquad (2)$$
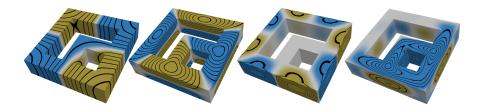
Fig. 2. Two eigenmodes of the lower spectrum on the double torus with sharp features, left: Laplacian, and right: modified Dirichlet energy.

where θ_{e_i} is the dihedral angle at the edge e_i, A_{e_i} is the combined area of the two triangles incident to e_i and $\|e_i\|$ is the length of the edge. The quantities $\|\bar{e}_i\|$, $\bar{A}_{e_i}$, and $\bar{\theta}_{e_i}$ are measured on the reference mesh. To write this flexural energy in the general form (1) we set

$$f_i = \theta_{e_i} \quad \text{and} \quad \omega_i = \frac{3\|e_i\|^2}{A_{e_i}}.$$

The membrane energy consists of two terms: one measuring the stretching of the edges,

$$E_L = \frac{1}{2} \sum_i \frac{1}{\|\bar{e}_i\|}(\|e_i\| - \|\bar{e}_i\|)^2, \tag{3}$$

and one measuring the change of the triangle areas A_i

$$E_A = \frac{1}{2} \sum_i \frac{1}{\bar{A}_i}(A_i - \bar{A}_i)^2. \tag{4}$$

Here the second sum runs over the triangles of the mesh. We can describe E_L in the general form (1) by setting

$$f_i = \|e_i\| \quad \text{and} \quad \omega_i = \frac{1}{\|e_i\|},$$

and to describe E_A we set

$$f_i = A_i \quad \text{and} \quad \omega_i = \frac{1}{A_i}.$$

3 Modes of Deformation Energies

Modal analysis provides ways to compute the modes of a surface with respect to a deformation energy. To inspect the modes of a mesh, given by a $3n$-vector $\bar{x}$, we consider a deformation energy $E(x)$ that has $\bar{x}$ as a reference surface. Then, we are interested in the eigenvalues and eigenmodes of the Hessian of the deformation energy E at the mesh $\bar{x} \in X$.

The Hessian of a deformation energy (or more general of a function) does not depend solely on the differentiable structure of X, but also on the metric on X, hence belongs to Riemannian geometry. Therefore, before considering the Hessian of E we equip X with a metric. Since X equals $\mathbb{R}^{3n}$, the tangent space $T_x X$ at a mesh x can be identified with $\mathbb{R}^{3n}$. We can interpret an element of $T_x X$ as a vector field on x, that assigns a vector in $\mathbb{R}^3$ to every vertex of x. Then, a natural choice of a scalar product on $T_x X$ is a discrete L^2-product, $e.g.$, the mass matrix used in FEM [28] or the discrete L^2-product used in DEC [5,27]. We denote the matrix, that describes the scalar product on $T_x X$ by M_x. For completeness, we would like to mention that if x is a mesh that has degenerate triangles, the discrete L^2-product on $T_x X$ may be only positive semi-definite. However, away from the closed set of meshes that have at least one degenerate triangle, X equipped with the discrete L^2-product is a Riemannian manifold.

We denote by ∂E_x the $3n$-vector containing the first partial derivatives of E at x and by $\partial^2 E_x$ the matrix containing the second partial derivatives at x. We would like to emphasize that ∂E_x and $\partial^2 E_x$ do not depend on the metric on X, whereas the gradient and the Hessian of E do. The gradient of E at x is given by

$$\operatorname{grad}_x E = M_x^{-1} \partial E_x. \tag{5}$$

The Hessian of E at a mesh x is the self-adjoint operator that maps any tangent vector $v \in T_x X$ to the tangent vector $\operatorname{hess}_x E(v) \in T_x X$ given by

$$\operatorname{hess}_x E(v) = \nabla_v \operatorname{grad}_x E, \tag{6}$$

where ∇ is the covariant derivative of X.

Hessian computation. In general, it is a delicate task to derive an explicit representation of the Hessian of a deformation energy and often only approximations of the Hessian are available. Here, we derive a simple explicit formula for the Hessian of a deformation in the general form (1) at the point $\bar{x}$, which involves only first derivatives of the f_i's.

Since the gradient of E vanishes at $\bar{x}$, one can show that at $\bar{x}$ the Hessian of E takes the following form

$$\operatorname{hess}_{\bar{x}} E = M_{\bar{x}}^{-1} \partial^2 E_{\bar{x}}.$$

Hence, at $\bar{x}$ we do not need derivatives of the metric to compute $\operatorname{hess}_{\bar{x}} E$. Furthermore, to compute the second partial derivatives of E at $\bar{x}$ we do not need to calculate second derivatives, but we only need the first derivatives of the f_i's. We present an explicit formula for $\partial^2 E_{\bar{x}}$ in the following Lemma.

Lemma 1 (Explicit Hessian). *Let E be a deformation energy of the form (1). Then, the matrix $\partial^2 E_{\bar{x}}$ containing the second derivatives of E at $\bar{x}$ has the form*

$$\partial^2 E_{\bar{x}} = \sum_i \omega_i(\bar{x}) \, \partial f_{i\,\bar{x}} \, \partial f_{i\,\bar{x}}^T, \tag{7}$$

where $\partial f_{i\,\bar{x}}^T$ denotes the transpose of the vector $\partial f_{i\,\bar{x}}$.
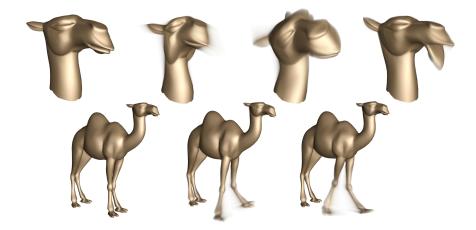
Fig. 3. Visualization of vibration modes derived from the discrete thin shell energy. In each row the left most image shows the rest state followed by some deformations captured by a vibration mode.

The computation of the first derivatives of the f_i's is usually straight forward, and, in addition, the first derivatives of many elementary quantities are explicitly stated in the literature. For example, a formula for the first derivative of the dihedral angle θ can be found in [28] and a formula for the first derivative of the area of a triangle is contained in [20].

Eigenvalue problem. To get the eigenmodes of $\mathrm{hess}_{\bar{x}}E$, we need to solve the generalized eigenvalue problem

$$\partial^2 E_{\bar{x}}\, \Phi = \lambda\, M_{\bar{x}}\, \Phi, \tag{8}$$

where $\Phi \in T_{\bar{x}}X$ and $\lambda \in \mathbb{R}$. The matrix $\partial^2 E_{\bar{x}}$ is symmetric and at least positive semi-definite ($\bar{x}$ is a minimum of E) and $M_{\bar{x}}$ is symmetric and positive definite. Hence, the structure of this problem is similar to the generalized eigenvalue problem arising in manifold harmonics [23, 27]. Fast solvers for this problem are discussed in [24, 27]. Since $\mathrm{hess}_{\bar{x}}E$ is self-adjoint with respect to the discrete L^2-product (given by $M_{\bar{x}}$), all eigenvalues of $\mathrm{hess}_{\bar{x}}E$, *i.e.* the solutions of (8), are real and the eigenmodes $\mathrm{hess}_{\bar{x}}E$ form an orthogonal basis of $T_{\bar{x}}X$. If we L^2-normalize the eigenmodes, they form an orthonormal basis of $T_{\bar{x}}X$ in which both Matrices $\partial^2 E_{\bar{x}}$ and $M_{\bar{x}}$ are diagonal matrices.

Vibration modes. To illustrate the concept of eigenmodes of the Hessian of a deformation energy, we look at the vibrations of a mesh in a force field induced by the energy. For simplicity, we consider the case of free vibrations. In general, the dynamics of a time-dependent mesh $x(t)$ in the space X is governed by a system of non-linear second-order ODEs of the form

$$M_{x(t)}\ddot{x}(t) = f(t, x(t), \dot{x}(t)),$$

see [1]. Here, the mass matrix M_x represents the physical mass of x and f represents the acting forces. We consider the force field that has E as its potential, *i.e.*,

$$f(t, x(t), \dot{x}(t)) = -\partial E_{x(t)}.$$

In the case of free vibrations, this is the only force. In a more general setting, we could include damping and exterior forces, see [18]. The equations that govern the motion of a time-dependent mesh $x(t)$ during free vibration are

$$\mathrm{grad}_{x(t)} E + \ddot{x}(t) = 0, \tag{9}$$

where we use the definition of the gradient, eq. (5), to simplify the formula. Since we are interested in meshes x that are (arbitrarily) close to $\bar{x}$, we expand the force $\mathrm{grad}_x E$ into a Taylor series around $\bar{x}$. Using $\partial E_{\bar{x}} = 0$ ($\bar{x}$ is a minimum of E) we get

$$\mathrm{grad}_x E = \mathrm{hess}_{\bar{x}} E(x - \bar{x}) + \mathcal{O}(\|x - \bar{x}\|^2). \tag{10}$$

Then, if we omit the second order term in (10) and plug (9) and (10) together, we get

$$\mathrm{hess}_{\bar{x}} E\, u(t) + \ddot{u}(t) = 0, \tag{11}$$

where $u(t) = x(t) - \bar{x}$. This is a system of second-order linear ODEs that are coupled by $\mathrm{hess}_{\bar{x}} E$. To solve the system we consider a normalized eigenbasis B of $\mathrm{hess}_{\bar{x}} E$. Written in such a basis, both matrices $\partial^2 E_{\bar{x}}$ and $M_{\bar{x}}$ are diagonal matrices and equation (11) takes the form

$$\Lambda\, w(t) + \ddot{w}(t) = 0, \tag{12}$$

where w is the representation of u in the basis B and Λ is a diagonal matrix that contains the eigenvalues. The system (12) is decoupled and can be solved row by row. Each row describes an oscillation around $\bar{x}$ with frequency $\sqrt{\lambda}$ in the direction of the eigenmode Φ corresponding to the eigenvalue λ. This means, that the eigenmodes of problem (8) describe the vibration modes of the mesh $\bar{x}$ (with respect to the deformation energy E).

   The vibrations of a physical system are usually not free, but are affected by damping forces. Common models for such forces are Rayleigh damping, see [12], and, even simpler, mass damping, see [18]. We would like to mention that if Rayleigh (or mass) damping forces are added to the system, it still has the same vibration modes, see [12].

Normal variations. In addition to arbitrary variations of the vertices of $\bar{x}$, we consider variations that restrict every vertex to vary only in direction of the surface normal at the vertex. Let us fix a normal direction at each vertex of the mesh. Then, a normal variation is determined by a function on the mesh. This reduces the eigenvalue problem (11) to an n-dimensional problem. We denote the restriction of $\partial^2 E_{\bar{x}}$ to the subspace of $T_{\bar{x}} X$ spanned by the vertex normals of $\bar{x}$ by $\partial^2 E_{\bar{x}}^N$. Then, equation (11) reduces to

$$\mathrm{hess}_{\bar{x}} E^N\, \varphi + \ddot{\varphi} = 0,$$
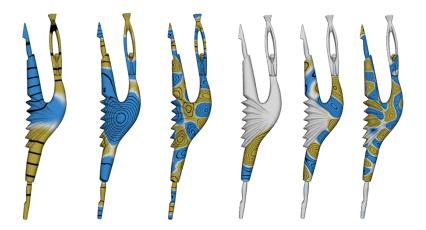
Fig. 4. Visualization of modes of the Laplacian (three images on the left) and modes of the thin shell energy restricted to normal variations (three images on the right).

where φ is a function on the mesh. The corresponding eigenvalue problem is

$$\partial^2 E_{\bar{x}}^N \, \varphi = \lambda \, M_{\bar{x}} \, \varphi,$$

where $M_{\bar{x}}$ is the mass matrix that represents the discrete L^2-product of functions on the mesh $\bar{x}$.

4   Quadratic Energies

In addition to energies defined on the space of meshes X, we consider energies that are defined on an appropriate space of functions on a surface. In particular, we consider the Dirichlet energy, that on a compact smooth surface Σ is defined for weakly differentiable functions $\varphi : \Sigma \to \mathbb{R}$ (that vanish at the boundary of Σ) by

$$E_\Delta(\varphi) = \frac{1}{2} \int_\Sigma \|\text{grad } \varphi\|^2 \, \mathrm{d}A. \tag{13}$$

This is an intrinsic energy, therefore, the energy and its eigenmodes do not change under isometric deformations of the surface Σ. For some applications this is a desired feature, for other applications it is not. By modifying the Dirichlet energy, we construct a new energy that is extrinsic.

Assume that Σ is an orientable surface in $\mathbb{R}^3$ and let ν denote the normal of Σ. Then, all three coordinates ν^k of ν are smooth functions and for a weakly differentiable function φ the product $\varphi \nu^k$ is weakly differentiable. We define

$$E_\Delta^N(\varphi) = \sum_{k=1}^3 E_\Delta(\varphi \, \nu^k). \tag{14}$$

This energy satisfies the equation

$$E_\Delta^N(\varphi) = E_\Delta(\varphi) + \frac{1}{2} \int_\Sigma \varphi^2 (\kappa_1^2 + \kappa_2^2) \mathrm{d}A, \tag{15}$$

where κ_1 and κ_2 are the principal curvatures of Σ. This means that $E_D^N(\varphi)$ is the sum of the Dirichlet energy of φ and the φ^2-weighted total curvature of Σ.

Discrete energies. In the discrete setting, we consider a mesh $x \in X$ and the space F_x of continuous functions $u : x \to \mathbb{R}$ that are linear in every triangle. Such a function is differentiable in the interior of every triangle, and hence one can directly evaluate the integral (13). For a rigorous treatment of this discrete Dirichlet energy and a convergence analysis see [7,13]. A function in F_x is already determined by its function values at the vertices of x, hence it can be represented by an n-vector. Then, the discrete Dirichlet energy E_D is a quadratic functional on F_x, and for a function $u \in F_x$ (represented by an n-vector) $E_D(u)$ is explicitly given by

$$E_D(u) = \frac{1}{2} u^T S u, \tag{16}$$

where S is the usual *cotan*-matrix, see [19,28].

To discretize the energy E_Δ^N we fix a normal direction at every vertex of the mesh, and we denote the oriented unit normal vector at a vertex v_i by $N(v_i)$. Then, we say a continuous and piecewise linear vector field V on x is a *normal vector field* if for every vertex v_i of x the vector $V(v_i)$ is parallel to $N(v_i)$. The space of normal vector fields on x is an n-dimensional vector space and the map that maps a function $u \in F_x$ to the normal variation V_u, given by $V_u(v_i) = u(v_i) N(v_i)$ for all $v_i \in x$, is a linear isomorphism. The three coordinate functions V_u^k of V_u are functions in F_x and we define the discrete energy E_D^N analog to eq. (14) by

$$E_D^N(u) = \sum_{k=1}^3 E_D(V_u^k).$$

A simple calculation shows that the energy E_D^N satisfies

$$E_D^N(u) = \frac{1}{2} u^T A u, \tag{17}$$

where the formula

$$A_{ij} = \langle N(v_i), N(v_j) \rangle S_{ij}$$

relates the entries A_{ij} of the matrix A to the entries S_{ij} of the cotan-matrix S.

The computation of the Hessian of the Dirichlet energy E_D and the energy E_D^N is simple. Both energies are quadratic, therefore the Hessian is constant and the matrices $\partial^2 E_D$ and $\partial^2 E_D^N$ are the matrices S and A given in equations (16) and (17). The metric we consider on F_x is the discrete L^2-product given by the mass matrix M. The eigenvalues and eigenfunctions of the Hessian of E_D (resp. E_D^N) satisfy the generalized eigenvalue problem $S\phi = \lambda M \phi$ (resp.

Fig. 5. Vibration distance to the marked vertex v of the Armadillo model in three colorings: continuous coloring from white being similar to red being dissimilar to v and binary colorings with two different thresholds where blue vertices are similar to v.

$A\phi = \lambda\, M\,\phi$). To abbreviate the terminology, we call these eigenvalues and eigenfunctions the eigenvalues and eigenmodes of the energy E_D (resp. E_D^N). Similar to the vibration modes of a deformation energy, the eigenmodes of E_D and E_D^N are orthogonal with respect to M. We would like to remark that the Hessian of the E_D is the discrete Laplace-Beltrami operator and therefore the eigenmodes and eigenvalues of E_D agree with the eigenfunctions and eigenvalues of the discrete Laplace-Beltrami operator.

Modes of E_D^N. As illustrated in Figures 1 and 2, the eigenmodes of E_D and E_D^N differ significantly. Whereas the eigenmodes of the Laplacian are insensitive to the extrinsic curvature, the modes of E_D^N corresponding to lower eigenvalues hardly move in regions of high curvature, see Fig 1. A possible explanation for this behavior is the following. The energy has its minimum at the origin of the space of normal vector fields. Therefore, at the origin the gradient of the energy vanishes and the modes of the Hessian corresponding to small eigenvalues point into directions of least expenditure of energy. Now, equation (15) shows that E_D and E_D^N differ by a zero's order term, that measures a weighted L^2-norm of the function, where the weight is the sum of the squared principal curvatures. Therefore, eigenmodes of E_D^N that correspond to small eigenvalues have small function values in areas of high curvature, because then a variation in this direction causes less increase of energy.

5   Modal Signatures

In this section we introduce two multi-scale surface signatures: the *vibration signature*, based on the vibration modes of the surface, and the *feature signature*, which uses the eigenfunctions and eigenvalues of the modified discrete Dirichlet energy E_D^N. The construction of the signatures follows the construction of the heat kernel signature defined in [26].

The signatures we consider are multi-scale signatures, which take a positive scale parameter t as input. For every t such a signature is a function on the mesh, *i.e.*, it associates a real value to every vertex of the mesh. Let v be a vertex of a mesh x and let t be a positive value. Then, we define the *vibration signature* of x at vertex v and scale t by

$$S_t^{Vib}(v) = \sum_j e^{-\lambda_j t} \left\| \Phi_j(v) \right\|^2 , \tag{18}$$

where λ_j and Φ_j denote the eigenvalues and the L^2-normalized vector-valued vibration modes of a mesh x. The value $\left\| \Phi_j(v) \right\|$ describes the displacement of the vertex v under the L^2-normalized vibration mode Φ_j. For a fixed t the vibration signature of v measures a weighted average displacement of the vertex over all vibration modes, where the weight of the jth eigenmode is $e^{-\lambda_j t}$. The weights depend on the eigenvalues and on the scale parameter. For increasing λ, the function $e^{-\lambda t}$ rapidly decreases, *e.g.*, the modes with smaller eigenvalue receive higher weights than the modes with large eigenvalues. Furthermore, for increasing t all weights decrease, and, more importantly, the weights of the vibration modes with smaller eigenvalues increases relative to the weights of the modes with larger eigenvalues.

The *feature signature* is constructed in a similar manner, but it uses the eigenmodes and eigenvalues of the modified Dirichlet energy E_D^N. We define

$$S_t^{Feat}(v) = \sum_j e^{-\lambda_j t} \phi_j(v)^2 \tag{19}$$

where the λ_j are the eigenvalues and the $\phi_j(v)$ are the L^2-normalized eigenmodes of the Hessian of the modified discrete Dirichlet energy E_D^N.

Multi-scale distances. From each of the two signatures we can construct the following (multi-scale) pseudo-metric on the mesh: let $v, \tilde{v}$ be vertices of the mesh x, then we define

$$\delta_{[t_1,t_2]}(v, \tilde{v}) = \left(\int_{t_1}^{t_2} \frac{(S_t(v) - S_t(\tilde{v}))^2}{\sum_k e^{-\lambda_k t}} \mathrm{d} \log t \right)^{\frac{1}{2}} . \tag{20}$$

By construction, for any pair of scale values $t_1 < t_2$, $\delta_{[t_1,t_2]}$ is positive semidefinite and symmetric, and one can show that it satisfies the triangle inequality. We call the pseudo-metrics constructed from S_t^{Vib} and S_t^{Feat} the *vibration distance* and the *feature distance*.

The idea behind the construction of the pseudo-metric is to use the integral $\int_{t_1}^{t_2} (S_t(v) - S_t(\tilde{v}))^2 \mathrm{d}t$. However, the actual definition additionally includes two heuristics. First, since for increasing t the values $S_t(v)$ decreases for all v, we normalize the value $(S_t(v) - S_t(\tilde{v}))^2$ by dividing it by the discrete L^1-norm of S_t,

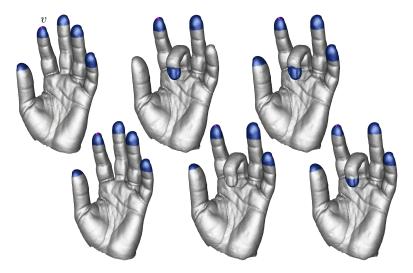$$\| S_t \|_{L^1} = \sum_k e^{-\lambda_k t}.$$

Fig. 6. Vertices (blue) similar to vertex v based on heat kernel signature [26] (top row) and our vibration signature (lower row). Left and right column depict similarity based on a small range of t's and middle column on a large range of t's.

Second, for a fixed vertex v the signature $S_t(v)$, in general, varies stronger for small values of t than for large t's. To increase the discriminative power of the pseudo-metric, we associate a higher weight to the small t's and a lower weight to the larger t's. We achieved this by using a weighted integral with weight function $\mathrm{dlog}\, t = \frac{1}{t}\mathrm{d}t$. To discretize this weighted integral we use a uniform decomposition of the logarithmically scaled interval $[t_1, t_2]$.

6 Results and Discussion

We experiment with the vibration modes of the discrete thin shell energy, the eigenmodes of E_D^N, and, for comparison, the eigenfunctions of the *cotan-* Laplace operator. In addition, we restrict the space of variations to normal variations of the mesh and inspect the modes of the thin shell energy in this setting. As a discrete L^2-scalar product we use the diagonal (or lumped) mass matrix M, which comes from FEM. The diagonal entry in the ith row of the matrix is a third of the combined area of the triangles adjacent to the ith vertex of the mesh. To compute the eigenmodes of a mesh, we solve the generalized eigenvalue problem (8). Since M is a diagonal matrix, this problem can be transformed into a standard eigenvalue problem as described in [27]. Then, we solve the resulting standard eigenvalue problem with the shift-and-invert Lanczos scheme described in [27]. For most examples and applications we do not need to compute the full spectrum, but only the lower part of the spectrum.
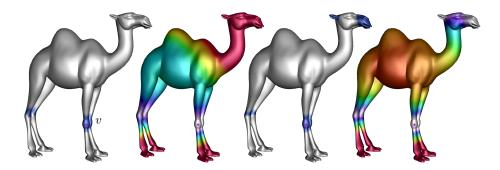
Fig. 7. Comparison of two similarity measures. Distance to vertex v in binary as well as continuous coloring based on our vibration signature (left most) and the heat kernel signature (right most).

Spectral zoo. We compare the eigenmodes of the Laplacian to the ones of the modified Dirichlet energy E_D^N and to the vibration modes of the thin shell energy restricted to normal variations. To convey an impression of the characteristics of the modes of the different energies, we show some examples in Figures 1, 2 and 4. To visualize the modes we use blue color for positive values, white for zero crossings, and orange for negative values. Additionally, we draw isolines as black lines.

As a first example, we study how the eigenmodes change when we isometrically deform a flat plate, see Fig. 1. On the undeformed flat plate, the eigenmodes of E_D^N equal the eigenmodes of the Laplacian. As shown in Fig. 1, there are certain differences between the three types of considered modes when computed on the deformed plate. Due to its intrinsic nature the Laplacian eigenmodes ignore the newly introduced feature, Fig. 1 left. In contrast, the eigenmodes of E_D^N and the vibration modes are sensitive to the feature, Fig. 1 middle and right. The eigenmodes of E_D^N corresponding to lower eigenvalues almost vanish at the feature and the vibration modes place additional extrema on the fold.

Investigating the differences between the eigenmodes of the Laplacian and E_D^N further, we compute them on the double torus with sharp features shown in Fig. 2. It can be seen that each of the shown Laplacian eigenmodes contains a more or less equally distributed set of extrema as well as a certain reflection symmetry, Fig. 2 left. The corresponding isolines suggest a low influence of the sharp features to the considered Laplacian eigenmodes. Similar to the Laplacian modes the two eigenmodes for E_D^N also posses a reflection symmetry, Fig. 2 right. But here we find that the eigenmodes of the lower part of the spectrum correspond to oscillations of flat areas surrounded by sharp edges, Fig. 2 right. This matches our considerations in Section 4.

For a third comparison, we choose a model without sharp edges, the dancer (25k vertices). We compare the eigenmodes of the Laplacian to the modes of the thin shell energy restricted to normal variations, see Fig. 4. As in the case of the torus we notice that the Laplacian eigenmodes oscillate equally over the whole
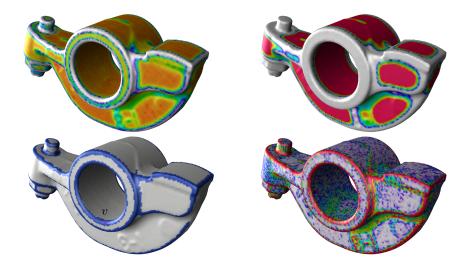
Fig. 8. Results of the feature signature on the rocker arm model. The top row shows the feature signature for increasing scale values. The bottom row shows on the left the feature distance to the marked vertex v binary colored by a threshold, and, on the right, the surface colored by curvature ($\sqrt{\kappa_1^2 + \kappa_2^2}$).

surface, see Fig. 4 left. In contrast, the vibration modes respect the extrinsic geometry features, *e.g.*, they align to the creases on the dancer model. In addition, on the dancer model vibration modes corresponding to the lower eigenvalues of the thin shell energy spectrum tend to concentrate on some parts of the surface, *e.g.*, a leg of the dancer. Though the whole surface vibrates, the amplitude of the vibration varies strongly across the surface.

Fig. 3 shows eigenvibrations with respect to the discrete thin shell energy. The images on the left (top and bottom row) show the reference mesh and each of the other images visualizes a vibration mode. The discrete thin shell energy is a weighted sum of a flexural and a membrane energy. If we decrease the weight of the membrane energy, the resulting vibration modes include stretching and squashing of the surface, Fig. 3 top row 2nd and 3rd image. In contrast, if we put a large weight on the membrane energy, the resulting eigenmodes try to preserve the metric. Examples of such modes are given in Fig. 3 top row 4th, bottom row 2nd and 3rd image.

Vibration Signature. In the following we examine the properties of the vibration signature S_t^{Vib} defined in eq. (18) and compare it to the heat kernel signature (HKS) introduced in [26]. As noted in Section 5, $S_t^{Vib}(v)$ encodes the vibration behavior of a vertex v on multiple scales, *i.e.*, vertices that oscillate with similar intensity throughout the eigenmodes, will be close in terms of the vibration distance $\delta_{[t_1,t_2]}(\cdot,\cdot)$. We illustrate this property in Fig. 5 for the Armadillo model (16k vertices). On the left we color plot the vibration distance
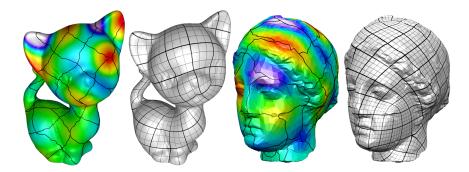
Fig. 9. Quadrangulation of the Kitten and the Venus model based on eigenmodes of the discrete thin shell energy restricted to normal variations.

$\delta_{[t_1,t_2]}(v,\cdot)$ to the marked vertex v. Two further binary colorings are given, colorizing vertices that are closer to v than a threshold in blue and the other vertices in white. For a small threshold the vertices on both feet are close to v; increasing the threshold causes parts of the hands to be colored in blue as well.

Fig. 6 compares S_t^{Vib} to the HKS. Every image of the hand model (40k vertices) depicts the vertices that are closer to the marked vertex v. In the first column similar results are achieved for HKS and S_t^{Vib}. Since the HKS is constructed using the spectrum and eigenfunctions of the Laplacian, the signature depends only on intrinsic properties of the surface. Thus the signature is incapable to discern isometrically deformed parts of a surface. The vibration signature however is sensitive to extrinsic information and hence represents an alternative to the HKS. This characteristic of S_t^{Vib} becomes especially apparent in the second column of Fig. 6. Here the middle finger of the hand is almost isometrically deformed. The HKS cannot distinguish this situation from the undeformed one; hence it recognizes the tips of the three longest fingers of the hand as similar to vertex v. As the deformation alters the vibration behavior of the bent finger, S_t^{Vib} detects only the tips of the unbent ones. Alike the HKS, the vibration distance can be evaluated at different scales (different choices of $[t_1,t_2]$). Choosing smaller t's increases the weights (*cf.* eq. 18) for eigenmodes with higher frequency. Therefore, more local vibrations described by these eigenmodes contribute more to the vibration distance. An example is shown on the right side of the lower row of Fig. 6. For smaller t's, $\delta_{[t_1,t_2]}(v,\cdot)$ captures vibrations of the fingertips as well and thus classifies the vertices on all tips as similar to v.

In Fig. 7 we provide a last comparison of the vibration signature and the HKS for the camel model (10k vertices). The vibration distance shown on the left, finds both pairs of knees (at the forelegs and at the hind legs) to be the closest to vertex v. For the HKS, shown on the right, the results are not as intuitive: the vertices at the mouth resp. ears of the camel are closer to the vertex v than the vertices at the hind legs, even closer than the vertices at the knees of the hind legs. This behavior of the HKS was the same at different scales and it is difficult to interpret the results. An indication for this behavior can be

found by inspecting the Fiedler vector, which is the eigenfunction of the discrete Laplacian associated to the lowest (non-zero) eigenvalue. Of all eigenfunctions, this one gets the highest weight in the signature. On the camel model, the Fiedler vector has one type of extrema (*e.g.* its minima) at tips of the toes of the hind legs at the tip of the tail and the other type of extrema (*e.g.* its maxima) at the tips of the toes of the forelegs, at the tips of the ears, and the tip of the snout. The function values at the tips of the ears and the tip of the snout are about the same as the function values at the knees of the forelegs. Hence, the contribution of this eigenfunction to the vibration distance is almost zero. This behavior repeats at some of the higher modes.

Feature Signature. The feature signature and the feature distance can be used to identify features of the surface like sharp bends or sharp corners. It is our impression that the signature could serve as an indicator function to surface segmentation algorithms. Fig. 8 shows the feature signature on the rockerarm model for different scale values. Vertices of the mesh that have a signature value close to zero are colored white in these images. The white areas seem to include the important features of the rocker arm model. The lower left image shows in blue all the vertices that are close (with respect to the feature distance) to a vertex on a sharp bend. For comparison we show a curvature plot ($\sqrt{\kappa_1^2 + \kappa_2^2}$) on the rocker arm.

Concerning the applicability as a feature indicator, an advantage of the feature signature over curvature is that the feature signature naturally comes with a scale parameter. Whereas the curvature is noisy and would require some smoothing operations, the feature distance even for low scale values seems to be much smoother. Another interesting difference is the following. Some areas of the rockerarm model have high curvature but do not indicate features, *e.g.*, the curved area inside the hole has a much higher curvature than for example the flat parts on the sides of the model. Still, the feature distance associates similar function values to both of these parts.

Quadrangulation. We investigate the applicability of the spectral quadrangulation approach by Dong et al. [6] to the eigenmodes of the thin shell energy restricted to normal variations. The Morse-Smale complex of an eigenfunction decomposes the surface into four-sided regions, see Fig. 9. Critical points emerging from high frequency noise in the functions are removed using *cancellations*, see Edelsbrunner et al. [8]. Based on the positions of the irregular (non valance 4) vertices and the connectivity of the Morse-Smale complex, a quadrangulation of the surface is constructed. The results of the quadrangulation algorithm for the Kitten (25k vertices) and the Venus (4k vertices) model are shown in Fig. 9. Two images are shown for every model: first the Morse-Smale complex together with the generating eigenmode and second the final quadrangulation. For the Kitten model the lines of the quadrangulation run diagonally while for the Venus the lines are aligned with the quadrilaterals of the Morse-Smale complex. Since the quadrangulation method depends on various factors, the initial function being only one of these, it is difficult to compare the results produced by eigenmodes of

the restricted thin shell energy to those of Laplacian eigenfunctions. Still, our impression is that the quadrangulations produced by eigenmodes of the restricted thin shell energy align more with the features of the surface.

7   Future Work

Using the eigenmodes of the thin shell energy restricted to normal variations for the quadrangulation of a surface yields promising results. Many critical points of the eigenmodes are placed on the characteristic features of the surface. In its current form the quadrangulation method varies the position of the critical points in order to produce quadrilaterals of similar size, and, therefore, moves the vertices of the quadrangulation away from the features. As future work we would like to modify this scheme such that the vertices of the quadrangulation are not allowed to move away from the feature, but still may vary along the feature. The goal would be to produce quadrangulations that include features (like sharp bends) of the surface. Furthermore, it would be interesting to include the feature signature into the quadrangulation process.

References

1. Baraff, D., Witkin, A.: Large steps in cloth simulation. In: Proceedings of ACM SIGGRAPH. pp. 43–54 (1998)
2. Barbič, J., James, D.L.: Real-time subspace integration for St. Venant-Kirchhoff deformable models. ACM Transactions on Graphics 24(3), 982–990 (2005)
3. Bridson, R., Marino, S., Fedkiw, R.: Simulation of clothing with folds and wrinkles. In: Proceedings of ACM SIGGRAPH/Eurographics Symposium on Computer Animation. pp. 28–36 (2003)
4. Choi, M.G., Ko, H.S.: Modal warping: Real-time simulation of large rotational deformation and manipulation. IEEE Transactions on Visualization and Computer Graphics 11(1), 91–101 (2005)
5. Desbrun, M., Hirani, A.N., Leok, M., Marsden, J.E.: Discrete exterior calculus (2005), `arXiv:math/0508341`, arXiv preprint
6. Dong, S., Bremer, P.T., Garland, M., Pascucci, V., Hart, J.C.: Spectral surface quadrangulation. ACM Transactions on Graphics 25(3), 1057–1066 (2006)
7. Dziuk, G.: Finite elements for the Beltrami operator on arbitrary surfaces. In: Partial Differential Equations and Calculus of Variations, Lecture Notes in Mathematics, vol. 1357, pp. 142–155. Springer (1988)
8. Edelsbrunner, H., Harer, J., Zomorodian, A.: Hierarchical Morse-Smale complexes for piecewise linear 2-manifolds. Discrete Computational Geometry pp. 87–107 (2003)
9. Garg, A., Grinspun, E., Wardetzky, M., Zorin, D.: Cubic Shells. In: Proceedings of ACM SIGGRAPH/Eurographics Symposium on Computer Animation. pp. 91–98 (Aug 2007)

10. Gebal, K., Bærentzen, J.A., Aanæs, H., Larsen, R.: Shape analysis using the auto diffusion function. Computer Graphics Forum 28(5), 1405–1413 (2009)
11. Grinspun, E., Hirani, A.N., Desbrun, M., Schröder, P.: Discrete shells. In: Proceedings of ACM SIGGRAPH/Eurographics Symposium on Computer Animation. pp. 62–67 (2003)
12. Hauser, K.K., Shen, C., O'Brien, J.F.: Interactive deformation using modal analysis with constraints. In: Graphics Interface. pp. 247–256 (2003)
13. Hildebrandt, K., Polthier, K., Wardetzky, M.: On the convergence of metric and geometric properties of polyhedral surfaces. Geometricae Dedicata 123, 89–112 (2006)
14. Huang, J., Zhang, M., Ma, J., Liu, X., Kobbelt, L., Bao, H.: Spectral quadrangulation with orientation and alignment control. ACM Transactions on Graphics 27(5), 1–9 (2008)
15. Huang, Q., Wicke, M., Adams, B., Guibas, L.: Shape decomposition using modal analysis. Computer Graphics Forum 28(2), 407–416 (2009)
16. Lévy, B., Zhang, H.: Spectral mesh processing. In: ACM SIGGRAPH ASIA Courses. pp. 1–47 (2009)
17. Ovsjanikov, M., Sun, J., Guibas, L.: Global intrinsic symmetries of shapes. Computer Graphics Forum 27(5), 1341–1348 (2008)
18. Pentland, A., Williams, J.: Good vibrations: modal dynamics for graphics and animation. In: Proceedings of ACM SIGGRAPH. pp. 215–222 (1989)
19. Pinkall, U., Polthier, K.: Computing discrete minimal surfaces and their conjugates. Experimental Mathematics 2(1), 15–36 (1993)
20. Polthier, K.: Computational aspects of discrete minimal surfaces. In: Hass, J., Hoffman, D., Jaffe, A., Rosenberg, H., Schoen, R., Wolf, M. (eds.) Global Theory of Minimal Surfaces. Clay Foundation (2005)
21. Reuter, M., Wolter, F.E., Peinecke, N.: Laplace-spectra as fingerprints for shape matching. In: Proceedings of the ACM Symposium on Solid and Physical Modeling. pp. 101–106 (2005)
22. Reuter, M., Wolter, F.E., Peinecke, N.: Laplace-Beltrami spectra as "Shape-DNA" of surfaces and solids. Computer-Aided Design 38(4), 342–366 (2006)
23. Rustamov, R.M.: Laplace-Beltrami eigenfunctions for deformation invariant shape representation. In: Proceedings of Eurographics/ACM SIGGRAPH Symposium on Geometry Processing. pp. 225–233 (2007)
24. Saad, Y.: Numerical Methods for Large Eigenvalue Problems. Manchester University Press (1992)
25. Sorkine, O., Alexa, M.: As-rigid-as-possible surface modeling. In: Proceedings of Eurographics/ACM SIGGRAPH Symposium on Geometry Processing. pp. 109–116 (2007)
26. Sun, J., Ovsjanikov, M., Guibas, L.J.: A concise and provably informative multi-scale signature based on heat diffusion. Computer Graphics Forum 28(5), 1383–1392 (2009)
27. Vallet, B., Lévy, B.: Spectral geometry processing with manifold harmonics. Computer Graphics Forum (2008)
28. Wardetzky, M., Bergou, M., Harmon, D., Zorin, D., Grinspun, E.: Discrete quadratic curvature energies. Computer Aided Geometric Design 24(8-9), 499–518 (2007)
29. Zhang, H., van Kaick, O., Dyer, R.: Spectral mesh processing. Computer Graphics Forum (2010), to appear